Nanoscale

PAPER

View Article Online
View Journal | View Issue

Cite this: *Nanoscale*, 2020, **12**, 18857

Directly measuring the structural transition pathways of strain-engineered VO_2 thin films†

Egor Evlyukhin, *[a] Sebastian A. Howard, [a] Hanjong Paik,[b,c] Galo J. Paez, [a] David J. Gosztola, [d] Christopher N. Singh, [a] Darrell G. Schlom,[b,e] Wei-Cheng Lee[a] and Louis F. J. Piper *[a]

Received 24th June 2020,
Accepted 1st September 2020

DOI: 10.1039/d0nr04776g

rsc.li/nanoscale

Epitaxial films of vanadium dioxide (VO_2) on rutile TiO_2 substrates provide a means of strain-engineering the transition pathways and stabilizing of the intermediate phases between monoclinic (insulating) M1 and rutile (metal) R end phases. In this work, we investigate structural behavior of epitaxial VO_2 thin films deposited on isostructural MgF_2 (001) and (110) substrates *via* temperature-dependent Raman microscopy analysis. The choice of MgF_2 substrate clearly reveals how elongation of V–V dimers accompanied by the shortening of V–O bonds triggers the intermediate M2 phase in the temperature range between 70–80 °C upon the heating–cooling cycles. Consistent with earlier claims of strain-induced electron correlation enhancement destabilizing the M2 phase our temperature-dependent Raman study supports a small temperature window for this phase. The similarity of the hysteretic behavior of structural and electronic transitions suggests that the structural transitions play key roles in the switching properties of epitaxial VO_2 thin films.

1. Introduction

Vanadium dioxide (VO_2) is a correlated electron material[1] and due to its exceptional switching properties is considered to be a promising candidate for metal–insulator-based electronics.[2,3] Bulk VO_2 undergoes a reversible, first-order, metal–insulator transition (MIT) at ~67 °C, which is conveniently near room temperature.[4–6] This transition has already been utilized in phase-change memristors for the purpose of novel biomimetic circuitry known as neuristors which have the potential to defy the scaling limitations of the metal–oxide–semiconductor field-effect transistors (MOSFETS) governed by Moore's Law.[7–9] Indeed, VO_2-based memristors, unlike MOSFETS, have a coherent transition throughout a singular material allowing devices to operate at nanometer scales.[10] Early studies showed that the MIT in VO_2 is accompanied by a structural phase transition (SPT) from the high-temperature rutile (R) phase to the low-temperature monoclinic (M1) phase.[11–13] During the SPT, upon cooling, vanadium chains zigzag and form V–V dimers along rutile c (c_R)-axis. It has been suggested that there are two major mechanisms responsible for VO_2 switching properties. The first mechanism is based on the electron–phonon interaction or Peierls instability[14] which is explained by the formation of V–V dimers along the rutile c_R-axis below the MIT temperature (T_{MIT}).[4] The second mechanism is the Mott transition[15] which suggests that the electron–electron correlation plays an important role in determining the transition pathway.[16] A consensus has emerged of a cooperative Mott–Peierls mechanism,[17–20] where strain-engineering the lattice can be used to enhance electron correlation strength and stabilize M2 and strongly correlated metallic phases due to the interplay between lattice, orbital and spin degrees of freedom.[21–23]

Previously, it has been demonstrated that epitaxial strain imposed on VO_2 thin films by their substrates, due to lattice mismatch can modify the T_{MIT} by ±40 °C depending on the substrate choice[24,25] and additionally, induce the formation of intermediate phases between M1 and R end phases.[21,23] For instance, compressive strain along c_R-axis lowers the T_{MIT} of epitaxial VO_2 thin films, whereas tensile strain along c_R-axis

[a]*Department of Physics, Applied Physics and Astronomy, Binghamton University, Binghamton, New York 13902, USA. E-mail: eevlyukh@binghamton.edu, lpiper@binghamton.edu*
[b]*Departments of Materials Science and Engineering, Cornell University, Ithaca, New York 14853-1501, USA*
[c]*Platform for the Accelerated Realization, Analysis and Discovery of Interface Materials (PARADIM), Cornell University, Ithaca, New York 14853, USA*
[d]*Center for Nanoscale Materials, Argonne National Laboratory, Lemont, Illinois 60439, USA*
[e]*Kavli Institute at Cornell for Nanoscale Science, Ithaca, New York 14853, USA*
†Electronic supplementary information (ESI) available. See DOI: 10.1039/d0nr04776g

raises the transition temperature to the metallic phase and the formation of an intermediate monoclinic insulating M2 phase between M1 and R phases is observed. The M2 phase is generally considered as a Mott insulator[26,27] in which only half of the vanadium atoms are dimerized.[18,28] It has been shown that this intermediate monoclinic structure can be stabilized in large single crystals by chemical doping[27,28] or by uniaxial pressure along $[110]_R$ direction.[26] More recently, stabilization of M2 phase has also been detected in VO_2 nanobeams subjected to the substrate-mediated strain and identified as a Mott insulating phase *via* direct charge carrier injection.[29,30] In the case of VO_2 thin films, the stabilization of M2 phase has been investigated from electronic excitation point of view *via* soft X-ray absorption spectroscopy.[21] However, the experimentally determined temperature window where M2 phase was found to be stable appeared to be quantitatively different than the theoretically predicted temperature range. This discrepancy has been explained in terms of increased electron correlation contributions as a result of the elongation of c_R-axis,[21] which facilitates the formation of the preemptive charge density waves.[31] Despite all of these findings, the stabilization mechanism and the effect of epitaxial strains on the formation of intermediate M2 phase in VO_2 thin films warrants further studies on how the local structure evolution is impacted by epitaxial strain.

Here, by using a direct local structural probe (Raman microscopy analysis) we investigate the interplay between strain effect and structural transition pathways as well as the local environment in epitaxial VO_2 thin films deposited on MgF_2 (001) and (110) substrates. Raman spectroscopy is a powerful tool for the investigation of structural and chemical transformations in organic/inorganic materials induced by temperature, pressure, doping, *etc*.[29,32,33] Although there have been many attempts to study SPT in VO_2 films by means of Raman spectroscopy,[25,34–36] the reported results were either not consistent (due to the large thicknesses of VO_2 films (80–100 nm)) or misinterpreted (due to the strong signal of the substrates). In our case, 10 nm thickness of the fabricated VO_2 thin films ensures the uniform character of applied epitaxial strains and therefore, the accuracy of the obtained results *via* Raman spectroscopy is significantly increased. Our analysis of the temperature-induced Raman shift of the characteristic peaks allows us to distinguish each of three phases (M1, M2, and R) during the SPT. We determine that in the (001) film, where c_R-axis is compressed, the intermediate phases are absent and only the M1–R transition is observed. Drastically, the (110) films with elongated c_R-axis exhibit stable intermediate M2 phase between the M1 and R endpoints in the temperature range between 70–80 °C upon heating and cooling steps. Furthermore, the observed gradual Raman shifts of the characteristic peaks during the SPT support previously suggested mechanism of temperature-induced structural transitions in VO_2 nanobeams *via* the formation of structural domains.[29,30] Finally, our studies provide new insight how Mott engineering of VO_2 thin films can be performed using epitaxial strain.

2. Experimental methods

High quality 10 nm-thick VO_2 films were grown on rutile MgF_2 (001) and (110) single crystal substrates by reactive molecular-beam epitaxy (MBE) *via* codeposition method under a distilled ozone background pressure at the PARADIM Thin Film Growth Facility at Cornell university.[37] The MIT transport measurements (resistance *vs.* temperature) were carried out using Quantum Design Physical Property Measurement System (Model 6000) at Cornell Center for Materials Research. The temperature-induced SPTs of epitaxially strained VO_2/MgF_2 (001) and (110) thin films were investigated by means of Raman microscopy analysis at the Center for Nanoscale Materials at the Argonne National Laboratory Raman spectra were recorded using a Raman microscope (*invia* Reflex, Renishaw, Inc.) with spectral resolution of 0.5 cm^{-1} using 532 nm excitation from a diode pumped solid state laser (RL532C50, Renishaw, Inc.). Samples were held in a nitrogen-purged temperature-controlled stage (THMS600/TMS94/LNP94, Linkam Scientific Instruments Ltd). Excitation and collection of scattered light occurred through a 50× objective (Leica, NA = 0.50). The laser power was set to 0.64 mW to exclude local heating effect. Collected spectra are typically consisted of averaging of 20 integrations (each integration was collected for 1 min). We note that at each temperature point several Raman spectra were collected and compared prior main measurement to assure the absence of local heating effect induced by a laser.

3. Results and discussion

The high quality of the films was verified by the MIT transport measurements (resistance *vs.* temperature) depicted in Fig. 1a.

Both films exhibit three orders of magnitude change in resistance upon heating and cooling steps, indicating the high quality of the films.[21,24,25,37] We also note that the (001) film is completely isotropic, whereas the (110) film exhibits anisotropy (see Fig. S1 (ESI†)). The T_{MIT} values equal to ~32 °C for (001) film and to ~72 °C for (110) film were taken at the midpoint of the jump in the resistance curve measured on heating. In the case of the (001) film the T_{MIT} is dramatically shifted to a lower temperature from that of a single crystal (67 °C), whereas the T_{MIT} of the (110) film is slightly shifted to a higher temperature and corresponding resistance curve exhibits a broader behavior demonstrating the effect of different types of substrate strains applied to the films. It has been previously shown that the T_{MIT} of VO_2 films strongly depends on the c_R-axis length. *i.e.* the V–V distance in the crystal lattice.[21,23–25] In a metallic state (rutile structure) vanadium atoms are lined up in the direction of the c_R-axis, thus with the decrease of c_R-axis the V–V distance is reduced. Respectively, the shortening of V–V distance leads to the overlapping of d orbitals which increases the width of d-band and stabilizes the metallic state of the rutile structure. Therefore, in the case of the (001) film when the contraction strain along c_R-axis is

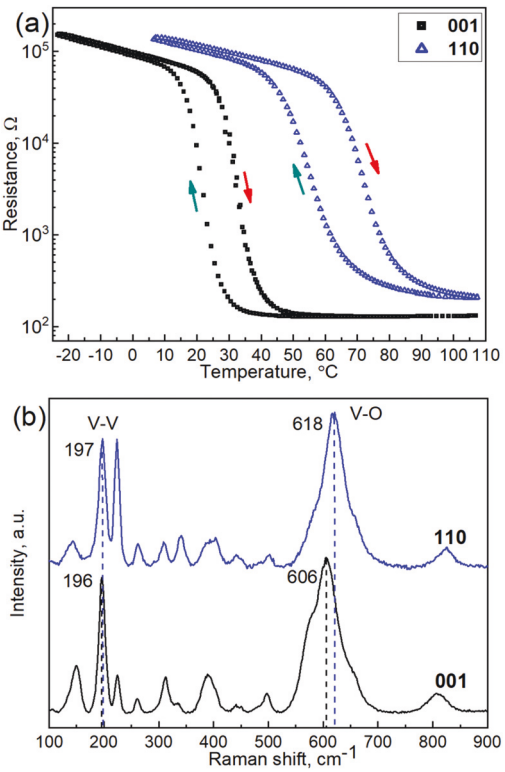

Fig. 1 (a) Temperature-dependent resistance measurements of 10 nm VO_2/MgF_2 (001) film (black squares) and 10 nm VO_2/MgF_2 (110) film (blue triangles). Red and green arrows indicate the heating and cooling steps correspondingly. (b) Raman spectra of VO_2/MgF_2 (001) and (110) thin films in the monoclinic M1 phase at 5 °C. Two main characteristic Raman peaks which represent V–V twisting vibrations and V–O bond vibrations are assigned with corresponding positions.[25,34,40]

applied the T_{MIT} is shifted to a lower temperature.[21,24] In contrast, tensile strain in the (110) films increases the T_{MIT}. We also note, that these changes of the T_{MIT} follows the same trend as for VO_2/TiO_2 thin films. However, the T_{MIT} values reported for VO_2 films deposited on TiO_2 substrates[24] where found to be smaller (~27 °C) in the case of (001) films and much larger (~96 °C) for (110) films than the T_{MIT} values obtained in this work. This difference can be explained by a larger lattice mismatch between VO_2 and MgF_2 substrates than in the case of VO_2/TiO_2 thin films,[25] thus VO_2/MgF_2 films, used in this work, were only partially strained (see Table S1 and Fig. S2(ESI†)). Nevertheless, the choice of MgF_2 substrates is defined by previous Raman spectroscopic measurements,[25] where it was shown that due to the intense Raman signal of the TiO_2 substrates the signal of VO_2 films is completely suppressed making Raman spectroscopy an inappropriate tool for investigating the temperature-induced SPT in VO_2/TiO_2 thin films.

The temperature-induced SPTs of epitaxially strained VO_2/MgF_2 (001) and (110) thin films were investigated by means of Raman microscopy analysis instead. Fig. 1b shows two Raman spectra of (001) and (110) thin films in monoclinic M1 phase collected at 5 °C. For (001) film the peaks are observed at 148, 196, 225, 260, 312, 334, 388, 496, 606 and 809 cm^{-1}. Respectively, for (110) film, Raman peaks are positioned at 144, 197, 223, 262, 308, 340, 393, 502, 618, and 826 cm^{-1}. In both cases, the relative position of M1 Raman peaks is consistent with previous reports[29,35,38,39] and only some degree of displacement is detected, indicating the effect of epitaxial strains imposed on the films. In VO_2 Raman spectra it is generally recognized that low-frequency peaks relate to V–V vibration modes, whereas those in a high-frequency region 300–700 cm^{-1} correspond to V–O bond vibrations.[40,41] Previously, for the unstrained VO_2, two characteristic peaks at 189–194 cm^{-1} and 221–223 cm^{-1} both with A_g symmetry were assigned to V–V vibration modes.[25,34] Particularly, the peak at 189–194 cm^{-1} represents the twisting vibration of the V–V dimers,[41,42] thus the spectral changes (position and intensity) of this peak can be used for characterization of the displacement motion of the vanadium atoms along c_R-axis.[25,35] The high-frequency Raman peak at 608–612 cm^{-1} (the unstrained VO_2 case) with A_g symmetry relates to the V–O vibrations[25,34] and it is generally viewed as a hallmark for the different VO_2 phases.[29,35] As it can be seen in Fig. 1b, in the case of (001) film the peak at 196 cm^{-1} is shifted toward higher frequencies in comparison to the relaxed VO_2. At the same time the peak at 606 cm^{-1} undergoes a shift toward lower frequencies relative to relaxed VO_2. These spectral displacements of two characteristic Raman peaks can be explained by the in-plane tensile strain of the MgF_2 (001) substrate imposed on VO_2 film. The in-plane tensile strain (elongation of V–O bonds) reduces the out-of-plane lattice constant which leads to the shortening of the distance between V–V dimers aligned along out-of-plane c_R-axis. Thus, in the (001) film Raman spectrum (see Fig. 1b) the shift of V–O peak to lower energy together with V–V peak shift to higher energy are observed. These observations are supported by our preliminary theoretical calculations of the lattice dynamics carried out within the density functional theory (DFT) with Perdew–Burke–Ernzerhof (PBE) approximation (see Fig. S3 (ESI†)).[43,44] In the case of (110) film the tensile strain along c_R-axis elongates the V–V dimer distance; therefore, it is appropriate to assume that the low-frequency Raman peaks should undergo a shift to lower energy relative to the relaxed VO_2. Nevertheless, as it can be seen in Fig. 1b the characteristic peaks which relate to both V–V and V–O vibrations are shifted toward higher frequencies. This unexpected Raman shift behavior of V–V peak can be explained by the biaxial nature of the epitaxial strain imposed on VO_2 film by MgF_2 (110) substrate. The tensile strain along c_R-axis elongates the V–V dimer distance and additional out-of-plane contraction strain shortens the V–O bonds.[22] The V–O shortening directly affects the twisting angle of V–V dimer vibrations, therefore, the significant increase of the intensity of the peak at 223 cm^{-1} and a shift to higher frequency of the peak positioned at 197 cm^{-1}, relative to the unstrained VO_2, are observed (see Fig. 1b). These strain-induced Raman peak shifts are in a good agreement with T_{MIT}-strain dependence discussed above.

With the aim of understanding the epitaxial strain effects on the temperature-induced SPT of VO_2/MgF_2 (001) and (110) thin films we performed temperature-controlled Raman spectroscopic measurements from 5–50 °C (in 2 °C increments) for the (001) film and from 5–90 °C for the (110) film correspondingly. Fig. 2a displays Raman spectra of VO_2/MgF_2 (001) film at selected temperature points upon heating. We note that at 50 °C no Raman signal from the film could be obtained due to the full transition of VO_2 to the metal state. Two different behaviors of low- and high-frequency phonon modes are recognized. Low-frequency Raman peak at 196 cm^{-1} (5 °C) which corresponds to V–V twisting vibrations shifts to about 191 cm^{-1} at 44 °C. During the cooling step, this peak reverts to its initial position (see Fig. S4 (ESI†)). The gradual decrease in frequency of V–V peak at 196 cm^{-1} upon heating reflects the elongation of V–V dimers induced by a thermal expansion of the crystal lattice.[35] Previously, it has been shown that in the metallic state, VO_2 exhibits the rutile structure and the vanadium atoms are equally positioned along c_R-axis with the interatomic distance equal to ~2.851 Å. Upon transitioning to the insulating M1 phase vanadium atoms form zigzag chains of V–V dimers along c_R-axis with corresponding dimers length (for unstrained VO_2) equal to ~2.654 Å.[7] Therefore, the observed shift of V–V peak is in a good agreement with previous studies, which showed that during the SPT of VO_2 from the M1 to R phase the elongation and rotation of V–V dimers along c_R-axis occurs.[7]

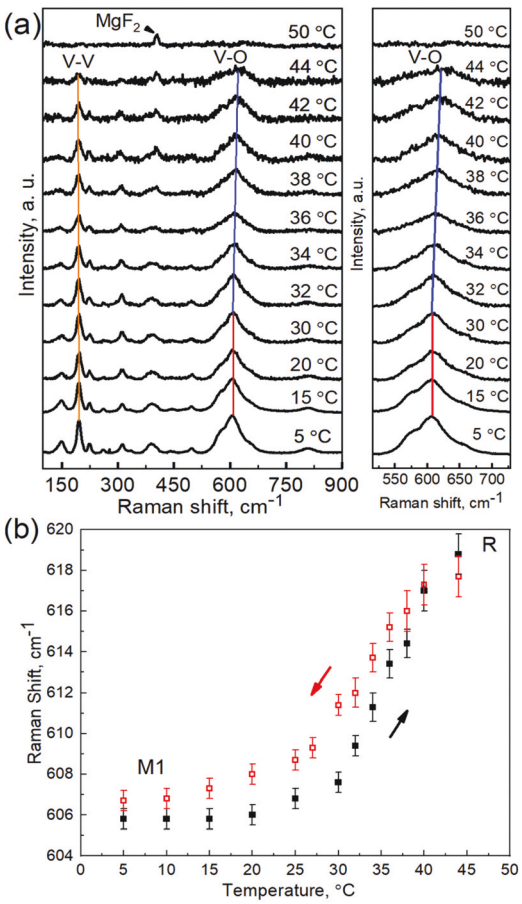

Fig. 2 (a) Raman spectra of VO_2/MgF_2 (001) at selected temperature points during heating. The range around 600 cm^{-1} is additionally depicted. Colored lines show the shift of characteristics Raman peaks. (b) Temperature-dependent Raman shift of V–O vibration mode upon heating (black squares) and cooling (open red squares). Each frequency value was obtained *via* Gaussian fittings.

The V–O vibrational modes at 606 cm^{-1} (5 °C) exhibit different transient behavior as a function of temperature. We investigated the temperature-dependent Raman shift evolution of V–O vibrations derived by Gaussian fittings of the corresponding peak (see Fig. 2b). Upon heating the stability of V–O Raman peak below 30 °C indicates that the entire (001) film is in the insulating M1 phase. In the temperature range between 30–44 °C a gradual increase in frequency is observed suggesting the shortening of V–O bonds in M1 phase. Furthermore, between 38–44 °C, a significant decrease of the signal-to-noise ratio and broadening of V–O peak are detected demonstrating the domination of the R phase over the monoclinic M1 phase. Above 44 °C, no Raman peaks can be recognized, indicating a complete transformation of the (001) film in to the metallic R phase. The structural transition pathway of (001) film is completely reversable upon cooling (see Fig. S5 (ESI†)). The same transient behaviour of V–V and V–O peaks during the temperature-induced SPT were observed for (011) VO_2 films deposited on the Na-based substrate with ZnO buffer layer.[45] Using Raman spectroscopic analysis Huang *et al.*[45] have observed similar spectral shifts toward lower and higher frequencies of V–V and V–O vibrational modes during the transition from the M1 to R phase, respectively. Moreover, the observed gradual temperature-induced Raman peaks shift supports previously suggested mechanism of SPT in VO_2 nanobeams *via* the formation of structural domains.[29]

The picture dramatically changes when the tensile strain along c_R-axis in (110) film is considered. Fig. 3a shows the temperature-dependent Raman measurements of VO_2/MgF_2 (110) thin film upon heating. The low-frequency Raman mode (V–V vibrations) positioned at 197 cm^{-1} (25 °C) remains stable during the heating up to 68 °C. Further increase of the temperature (68–70 °C) induces a shift to higher frequency (relaxation of twisting of V–V dimers)[35] to about 201 cm^{-1} where it stays stable until 80 °C (see Fig. S6 (ESI†)). On the other hand, the high-frequency Raman peak (V–O vibrations) positioned at 618 cm^{-1} (25 °C) upon heating to 55 °C does not undergo any spectral displacement. The gradual shift of this peak to about 641 cm^{-1} is observed in the temperature range between 55–70 °C representing the elongation of V–O bonds. Further increase of the temperature from 70 °C to 80 °C does not induced any spectral shift of V–O peak demonstrating the structural stability of the (110) film in this temperature range. Both low- and high-frequency Raman peaks shift toward the corresponding Raman peaks of M2 phase before complete disappearance.[29,35,40] Above 80 °C the noise level is dramatically increased and no Raman peaks can be detected. Upon cooling both Raman peaks return to their initial positions at

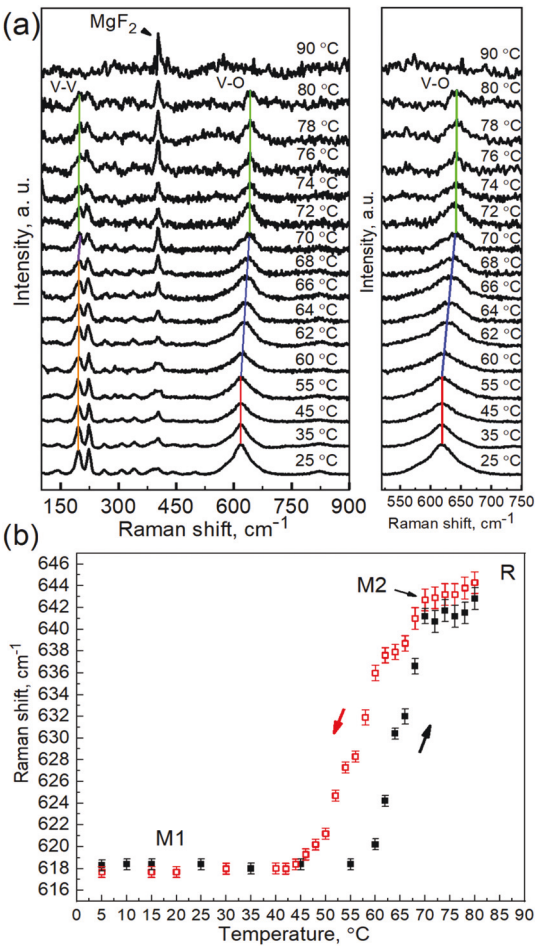

Fig. 3 (a) Raman spectra of VO_2/MgF_2 (110) at selected temperature points during heating. The range around 600 cm^{-1} is additionally depicted. Colored lines show the shift of characteristics Raman peaks. (b) Temperature-dependent Raman shift of V–O vibration mode upon heating (black squares) and cooling (open red squares). Each frequency value was obtained *via* Gaussian fittings.

slightly different temperatures due to the hysteresis effect (see Fig. S7 (ESI†)).

Previously, it has been shown that in the M2 phase only half of the vanadium atoms are dimerized whereas the other half reserves the zigzag type deviations.[7] Therefore, the observed temperature-induced frequency increase of V–V phonon modes, upon heating from 197–201 cm^{-1} suggests the structural transition of (110) film from M1 to M2 phase. This observation is supported by the temperature induced evolution of the high-frequency Raman peak (V–O vibration modes). Fig. 3b shows the values of V–O phonon mode frequency at different temperature points during the heating–cooling cycle which was derived by Gaussian fitting. At temperatures between 5–55 °C (upon heating) the entire film is in the M1 phase. Upon further heating (55–70 °C) a gradual shift is detected, suggesting the formation of M2 and R structural domains.[29] At 70 °C the M1 phase is completely consumed by M2 and R phases and only Raman spectra of the M2 phase is detected. The following plateau between 70–80 °C indicates the temperature range where the M2 phase is stable. Nevertheless, the increased level of noise and broadening of characteristic Raman peaks (see Fig. 3a) suggest the continues formation of R domains between 70–80 °C. Above 80 °C the entire film is transformed in to the metallic R phase. Upon cooling the structural pathway is found to be identical only with slight variations of the transition temperatures, which can be explained by the different symmetry of the monoclinic M1 and tetragonal R starting phase points. The nucleation of M2 phase is most likely due to the tensile strain along c_R-axis of (110) MgF_2 substrate. The applied tensile strain along c_R-axis elongate V–V dimers and significantly facilitate the temperature-induced reorganization of vanadium atoms. Moreover, the additional in-plane contraction strain induced by (110) MgF_2 substrate shortens the V–O bonds and breaks the symmetry of VO_2 films. Thus, half of the vanadium atoms become strongly paired along c_R-axis and the other half form zigzag chains along the same direction. These findings are in a good agreement with early work regarding VO_2 single crystals, where the formation and stabilization of the M2 phase was demonstrated upon application of a $[110]_R$ uniaxial compressive stress.[26] Moreover, our previous studies using X-ray absorption spectroscopy indirectly revealed that the stability of the M2 phase is significantly destabilized compared to thermodynamic predictions because of enhanced electron correlation.[21] That was an unexpected result since the M2 phase is commonly agreed upon as the fingerprint of Mott physics for VO_2. Therefore, the obtained small temperature window (~10 °C) where the M2 phase is stable supports our proposed M2 destabilisation mechanism *via* increased electron correlation due to the elongation of c_R-axis,[21] which facilitates the formation of the preemptive charge density waves.[31]

The hysteretic behavior of temperature induced structural changes of both VO_2/MgF_2 (001) and (110) films (see Fig. 2b and 3b) is found to be quite similar to the electrical transport measurements displayed on Fig. 1a. Although, the structural transition pathways for both films were found to be different, due to various strain effects, the excellent correspondence of the SPT and MIT transition temperatures as well as the Raman spectra evolution along the MIT suggest that the structural transitions play key roles in switching behavior of epitaxially strained VO_2 thin films.

4. Conclusions

In summary, by using Raman spectroscopy we investigated the temperature-induced structural evolution of epitaxial VO_2/MgF_2 (001) and (110) thin films. The strong epitaxial strain dependence on the structural transition pathways was demonstrated. We showed that upon heating–cooling cycle the VO_2/MgF_2 (001) undergoes a reversible structural transition from the insulating M1 phase to the metallic R phase. In contrast, the structural transition of VO_2/MgF_2 (110) was found to proceed *via* the formation of the intermediate insulating M2

phase between M1 and R end phases. Moreover, the temperature range where the M2 phase is stable was identified within a small window between 70–80 °C. Finally, the similarity between VO_2 structural behavior and the hysteretic metal–insulator transition suggests the key role of the structural transitions in resistive switching properties of VO_2.

Conflicts of interest

There are no conflicts to declare.

Acknowledgements

We thank Dr Benjamin T. Diroll for assistance with Raman microscopy measurements. This paper is based on the work supported by the Air Force Office of Scientific Research under Award No. FA9550-18-1-0024 administered by Dr Ali Sayir. For the film synthesis we acknowledge the National Science Foundation (Platform for the Accelerated Realization, Analysis, and Discovery of Interface Materials (PARADIM)) under Cooperative Agreement No. DMR-1539918. This research used resources of the Center for Nanoscale Materials, an Office of Science user facility, was supported by the U.S. Department of Energy, Office of Science, Office of Basic Energy Sciences, under Contract No. DE-AC02-06CH11357. Moreover, this work made use of the Cornell Center for Materials Research Shared Facilities which are supported through the NSF MRSEC program (DMR-1719875). Galo J. Paez acknowledges doctoral degree grant support (Grant No. E0565514) from the Comisión Fulbright Ecuador in conjunction with the Ecuadorian National Science Department Secretaría de Educación Superior, Ciencia, Tecnología e Innovación (Senescyt).

References

1 J. Cao, E. Ertekin, V. Srinivasan, W. Fan, S. Huang, H. Zheng, J. W. L. Yim, D. R. Khanal, D. F. Ogletree, J. C. Grossman and J. Wu, *Nat. Nanotechnol.*, 2009, **4**, 732–737.
2 N. Shukla, A. V. Thathachary, A. Agrawal, H. Paik, A. Aziz, D. G. Schlom, S. K. Gupta, R. Engel-Herbert and S. Datta, *Nat. Commun.*, 2015, **6**, 7812.
3 T. Yajima, T. Nishimura and A. Toriumi, *Nat. Commun.*, 2015, **6**, 10104.
4 J. B. Goodenough, *J. Solid State Chem.*, 1971, **3**, 490–500.
5 F. J. Morin, *Phys. Rev. Lett.*, 1959, **3**, 34–36.
6 V. Eyert, *Phys. Rev. Lett.*, 2011, **107**, 016401.
7 J. L. Andrews, D. A. Santos, M. Meyyappan, R. S. Williams and S. Banerjee, *Trends Chem.*, 2019, **1**, 711–726.
8 W. Yi, K. K. Tsang, S. K. Lam, X. Bai, J. A. Crowell and E. A. Flores, *Nat. Commun.*, 2018, **9**, 4661.
9 J. Lappalainen, J. Mizsei and M. Huotari, *J. Appl. Phys.*, 2019, **125**, 044501.
10 M. Nakano, K. Shibuya, D. Okuyama, T. Hatano, S. Ono, M. Kawasaki, Y. Iwasa and Y. Tokura, *Nature*, 2012, **487**, 459–462.
11 A. Cavalleri, T. Dekorsy, H. H. W. Chong, J. C. Kieffer and R. W. Schoenlein, *Phys. Rev. B: Condens. Matter Mater. Phys.*, 2004, **70**, 161102.
12 S. Biermann, A. Poteryaev, A. I. Lichtenstein and A. Georges, *Phys. Rev. Lett.*, 2005, **94**, 026404.
13 R. M. Wentzcovitch, W. W. Schulz and P. B. Allen, *Phys. Rev. Lett.*, 1994, **72**, 3389–3392.
14 E. Pytte, *Phys. Rev. B: Solid State*, 1974, **10**, 4637–4642.
15 N. F. Mott, *Proc. Phys. Soc., London, Sect. A*, 1949, **62**, 416–422.
16 A. Zylbersztejn and N. F. Mott, *Phys. Rev. B: Solid State*, 1975, **11**, 4383–4395.
17 T. M. Rice, H. Launois and J. P. Pouget, *Phys. Rev. Lett.*, 1994, **73**, 3042.
18 V. Eyert, *Ann. Phys.*, 2002, **11**, 605–704.
19 T. C. Koethe, Z. Hu, M. W. Haverkort, C. Schüßler-Langeheine, F. Venturini, N. B. Brookes, O. Tjernberg, W. Reichelt, H. H. Hsieh, H. J. Lin, C. T. Chen and L. H. Tjeng, *Phys. Rev. Lett.*, 2006, **97**, 116402.
20 G. J. Paez, C. N. Singh, M. J. Wahila, K. E. Tirpak, N. F. Quackenbush, S. Sallis, H. Paik, Y. Liang, D. G. Schlom, T.-L. Lee, C. Schlueter, W.-C. Lee and L. F. J. Piper, *Phys. Rev. Lett.*, 2020, **124**, 196402.
21 N. F. Quackenbush, H. Paik, M. J. Wahila, S. Sallis, M. E. Holtz, X. Huang, A. Ganose, B. J. Morgan, D. O. Scanlon, Y. Gu, F. Xue, L. Q. Chen, G. E. Sterbinsky, C. Schlueter, T. L. Lee, J. C. Woicik, J. H. Guo, J. D. Brock, D. A. Muller, D. A. Arena, D. G. Schlom and L. F. J. Piper, *Phys. Rev. B*, 2016, **94**, 085105.
22 S. Mukherjee, N. F. Quackenbush, H. Paik, C. Schlueter, T. L. Lee, D. G. Schlom, L. F. J. Piper and W. C. Lee, *Phys. Rev. B*, 2016, **93**, 241110.
23 W. C. Lee, M. J. Wahila, S. Mukherjee, C. N. Singh, T. Eustance, A. Regoutz, H. Paik, J. E. Boschker, F. Rodolakis, T. L. Lee, D. G. Schlom and L. F. J. Piper, *J. Appl. Phys.*, 2019, **125**, 082539.
24 Y. Muraoka and Z. Hiroi, *Appl. Phys. Lett.*, 2002, **80**, 583–585.
25 K. Shibuya, J. Tsutsumi, T. Hasegawa and A. Sawa, *Appl. Phys. Lett.*, 2013, **103**, 021604.
26 J. P. Pouget, H. Launois, J. P. D'Haenens, P. Merenda and T. M. Rice, *Phys. Rev. Lett.*, 1975, **35**, 873–875.
27 J. P. Pouget, H. Launois, T. M. Rice, P. Dernier, A. Gossard, G. Villeneuve and P. Hagenmuller, *Phys. Rev. B: Solid State*, 1974, **10**, 1801–1815.
28 M. Marezio, D. B. McWhan, J. P. Remeika and P. D. Dernier, *Phys. Rev. B: Solid State*, 1972, **5**, 2541–2551.
29 S. Zhang, J. Y. Chou and L. J. Lauhon, *Nano Lett.*, 2009, **9**, 4527–4532.
30 J. I. Sohn, H. J. Joo, D. Ahn, H. H. Lee, A. E. Porter, K. Kim, D. J. Kang and M. E. Welland, *Nano Lett.*, 2009, **9**, 3392–3397.

31 C. N. Singh, L. F. J. Piper, H. Paik, D. G. Schlom and W.-C. Lee, 2020, arXiv: 2005.02957.
32 E. Evlyukhin, E. Kim, D. Goldberger, P. Cifligu, S. Schyck, P. F. Weck and M. Pravica, *Phys. Chem. Chem. Phys.*, 2018, **20**, 18949–18956.
33 E. Evlyukhin, L. Museur, M. Traore, C. Perruchot, A. Zerr and A. Kanaev, *Sci. Rep.*, 2015, **5**, 18244.
34 G. I. Petrov, V. V. Yakovlev and J. Squier, *Appl. Phys. Lett.*, 2002, **81**, 1023–1025.
35 K. Okimura, N. H. Azhan, T. Hajiri, S. I. Kimura, M. Zaghrioui and J. Sakai, *J. Appl. Phys.*, 2014, **115**, 153501.
36 M. Yang, Y. Yang, B. Hong, L. Wang, K. Hu, Y. Dong, H. Xu, H. Huang, J. Zhao, H. Chen, L. Song, H. Ju, J. Zhu, J. Bao, X. Li, Y. Gu, T. Yang, X. Gao, Z. Luo and C. Gao, *Sci. Rep.*, 2016, **6**, 23119.
37 H. Paik, J. A. Moyer, T. Spila, J. W. Tashman, J. A. Mundy, E. Freeman, N. Shukla, J. M. Lapano, R. Engel-Herbert, W. Zander, J. Schubert, D. A. Muller, S. Datta, P. Schiffer and D. G. Schlom, *Appl. Phys. Lett.*, 2015, **107**, 163101.
38 P. Schilbe and D. Maurer, *Mater. Sci. Eng., A*, 2004, **370**, 449–452.
39 J. C. Parker, *Phys. Rev. B: Condens. Matter Mater. Phys.*, 1990, **42**, 3164–3166.
40 C. Marini, E. Arcangeletti, D. Di Castro, L. Baldassare, A. Perucchi, S. Lupi, L. Malavasi, L. Boeri, E. Pomjakushina, K. Conder and P. Postorino, *Phys. Rev. B: Condens. Matter Mater. Phys.*, 2008, **77**, 235111.
41 M. Nazari, Y. Zhao, V. Hallum, A. A. Bernussi, Z. Y. Fan and M. Holtz, *Appl. Phys. Lett.*, 2013, **103**, 043108.
42 B. Y. Qu, H. Y. He and B. C. Pan, *J. Appl. Phys.*, 2011, **110**, 113517.
43 J. P. Perdew, K. Burke and M. Ernzerhof, *Phys. Rev. Lett.*, 1996, **77**, 3865–3868.
44 J. P. Perdew, K. Burke and M. Ernzerhof, *Phys. Rev. Lett.*, 1997, **78**, 1396.
45 Y. Huang, D. Zhang, Y. Liu, J. Jin, Y. Yang, T. Chen, H. Guan, P. Fan and W. Lv, *Appl. Surf. Sci.*, 2018, **456**, 545–551.